Applied Catalysis B: Environmental 312 (2022) 121437

Contents lists available at ScienceDirect

Applied Catalysis B: Environmental

journal homepage: www.elsevier.com/locate/apcatb

Efficient low-temperature hydrogenation of fatty acids to fatty alcohols and alkanes on a Ni-Re bimetallic catalyst: The crucial role of NiRe alloys

Xincheng Cao [a,b,d,e], Jiaping Zhao [a,b,d,e], Feng Long [a,b,d,e], Peng Liu [a,b,d,e], Xia Jiang [a,b,d,e], Xiaolei Zhang [c], Junming Xu [a,b,d,e,f,*], Jianchun Jiang [a,b,d,e,f,*]

[a] Institute of Chemical Industry of Forest Products, Chinese Academy of Forestry, SFA, Nanjing 210042, China
[b] Key and Open Lab. on Forest Chemical Engineering, SFA, Nanjing 210042, China
[c] Department of Chemical and Process Engineering, University of Strathclyde, UK
[d] National Engineering Lab. for Biomass Chemical Utilization, SFA, Nanjing 210042, China
[e] Key Lab. of Biomass Energy and Material, SFA, Nanjing, Jiangsu Province 210042, China
[f] Co-Innovation Center of Efficient Processing and Utilization of Forest Resources, Nanjing Forestry University, China

ARTICLE INFO

Keywords:
Selective hydrogenation
Low-temperature conversion
Ni-Re bimetallic catalyst
Fatty alcohols

ABSTRACT

Selective hydrogenation of fatty acids is important for production of sustainable fuels and valuable chemicals as well as for the utilization of natural oils and fats. Generally, high reaction temperature (>200 °C) is required due to the weak polarizability and low reactivity of the carbonyl group of fatty acids. Here, we report an efficient catalytic system (Ni-Re/SBA-15 bimetallic catalyst) that realizes the low-temperature conversion of fatty acids to corresponding alcohols (reaction temperature: 150 °C) and diesel-range alkanes (170 °C) with high yields, surpassing the catalytic performance rendered by most of the catalytic systems reported so far. Detailed investigation into the nature of the catalyst showed that the superior activity originated from the formation of NiRe alloy, which improved the dispersion of metallic Ni, the H_2 activation ability and promoted the fatty acids/alcohols adsorption on the catalyst surface at low temperatures. More importantly, due to its strong electrophilicity, the fatty acids with highly electronegative carbonyl oxygen can be preferentially adsorbed on the catalyst surface than the fatty alcohols, which leads fatty acids to be converted preferentially. In this way, high catalytic efficiency and fatty alcohol selectivity can be obtained at a low temperature (150 °C). Further increasing reaction temperature to 170 °C, the reactant can be hydrodeoxygenated to form diesel-range alkanes. This developed NiRe/SBA-15 catalytic system highlights a great prospect for production of valuable fatty alcohols and alkanes from the conversion of bioderived fatty acids under mild conditions.

1. Introduction

Bio-feedstocks rich in fatty acids and triglycerides such as natural oils and fats are promising for producing the liquid biofuels and valuable chemicals [1,2]. Recent years, vegetable oils and waste cooking oils are being used as a low-cost renewable resources to produce the diesel-range alkanes, known as the second-generation biodiesel, or the fatty alcohols that are important compounds for plasticizer, cosmetic and lubricant productions [3–5]. For the production of diesel-range alkanes or fatty alcohols, currently, commercial metal sulfide ($NiMoS_4$ and $CoMoS_4$) [6,7] or copper-chromite ($CuO/CuCr_2O_4$) [8] catalysts have been developed and applied for the hydrogenation of natural oils. However, harsh reaction conditions (200–400 °C and high H_2 pressure) and the introduction of toxic S or Cr elements greatly limited their application [9,10].

In order to develop a highly efficient and environmentally friendly catalyst for the selective hydrogenation of component of natural oils, at present, researches are mainly focused on the precious metal or their derived bimetallic catalysts [11–13]. For instance, Liu et al. [11] proposed that the synergy between the Ir metal and partially reduced ReO_x can effectively promote the conversion of vegetable oils to diesel-range alkanes at low temperature (180 °C). Although these catalysts exhibited high catalytic activities for the hydrogenation of lipids and their model compounds, it would be desirable to find an abundant and economic catalysts that can still work at a low reaction temperature and H_2 pressure. In this respect, metallic Ni is a promising for the hydrogenation

* Corresponding authors at: Institute of Chemical Industry of Forest Products, Chinese Academy of Forestry, SFA, Nanjing 210042, China.
E-mail addresses: xujunming@icifp.cn (J. Xu), bio-energy@163.com (J. Jiang).

https://doi.org/10.1016/j.apcatb.2022.121437
Received 16 January 2022; Received in revised form 13 April 2022; Accepted 18 April 2022
Available online 22 April 2022

of natural oils. However, it exhibits weak hydrogenation activity at low temperature and high C-C bond hydrogenolysis activity at high temperatures, which result in a low product yield. To improve catalyst activity and suppress the occurrence of the side reactions caused by the single metallic Ni, a feasible strategy is to construct Ni-based alloy or intermetallic compound (IMC). Since the introduced second metal can provide geometric and /or electronic modification to the metallic Ni [14,15]. In prior works, NiIn IMC [16], NiCu [5,17] and NiFe alloys [18] have been reported and exhibited remarkably results for the synthesis of fatty alcohols and alkanes from the conversion of fatty acids. Although these catalysts showed high target product selectivity, high reaction temperatures ($\geq$ 250 °C) are still required due to the decreasing catalytic activity. Therefore, developing a catalyst system with high activity and product selectivity is highly demand for the conversion of fatty acids.

Rhenium species (Re metal or ReO_x) have been widely employed in the conversion of biomass oxygen-containing compounds due to its strong oxophilicity activity [19–21]. In particular, the combination of Re species with noble metals (Pd, Ir or Ru) are efficient for the hydrogenation of fatty acids due to the synergy between the noble metal (Pd, Ir or Ru) and partially reduced ReO_x species [11,22,23]. As compared to combination of Re species with noble metals, however, few researches on the NiRe bimetallic catalysts for the hydrogenation of fatty acids, and their intrinsic activities are not revealed. One important reason may be that the reduction of NiRe catalysts requires a high reduced temperatures (> 400 °C) owing to the reduction of NiO to metallic Ni, which results in the Re species mainly existing in the form of metallic Re instead of ReO_x on the catalyst surface. Compared with the partially reduced ReO_x species which are rich in unsaturated active sites (Re^{2+}, Re^{3+}, Re^{4+}, Re^{6+}), metallic Re (Re^0) is difficult to be used as an effective active metal assistant to promote the conversion of reactant under mild conditions due to its relatively low oxophilicity activity.

In this work, we reported that after reduction at high temperature (500 °C) in a H_2 flow, the NiRe alloys formed on the surface of the bimetallic catalysts can efficiently catalyze fatty acids conversion into fatty alcohols or diesel-range alkanes at low temperatures (150–170 °C). Compared with the previously reported combination of noble metal and partially reduced ReO_x catalytic system, the developed NiRe bimetallic catalysts not only show similar or even higher catalytic activity for the hydrogenation of fatty acids, but also exhibit tunable selectivity towards fatty alcohol and diesel-range alkane products. In order to promote the dispersion of metal active sites, mesoporous silica material of SBA-15 was selected as catalyst support because of its high surface areas and good thermal stability [24–26]. Detailed characterization (XRD, H_2-TPR, XPS and CO-FTIR) were performed to probe catalyst structure and possible electronic interaction between the Ni and Re in the bimetallic catalyst. In-situ FTIR of octanoic acid and DFT calculations were conducted to elaborate its high catalyst activity at low temperature and reveal the underlying structure-activity relationship. Additionally, the several crucial parameters, such as the Ni/Re molar ratio, reaction temperature, H_2 pressure and catalyst stability, were also investigated.

2. Experimental section

2.1. Chemicals

$Ni(NO_3)_2{\cdot}6H_2O$ (purity, 98.0%), NH_4ReO_4 (purity, 99.9%), $(NH_4)_6Mo_7O_{24}{\cdot}4H_2O$ (purity, 99.5%), $Fe(NO_3)_3{\cdot}9H_2O$ (purity, 98.5%) were purchased from Macklin (Shanghai, China). SBA-15 (BET surface area, 550–600 m^2/g, pore size: 6–11 nm) were purchased from XFNANO (Jiangsu, China). All chemicals were used without further purification.

2.2. Catalyst preparation

The supported Ni_xRe_y bimetallic catalysts with different molar ratio were synthesized by co-impregnation method, where x and y refer to the molar ratio of the metal atom. Typically, a calculated amounts of Ni $(NO_3)_2.6\ H_2O$ and NH_4ReO_4 were added into the solution containing SBA-15 support. After impregnation for 12 h, the obtained samples were dried at 80 °C for 10 h and then calcined at 400 °C for 5.0 h in air. The amount of Ni loading related to the support was fixed at 10 wt% while the Re loading was varied. Detailed amounts of metal loading were displayed in Table S1. As for the monometallic catalysts of Ni_1 and Re_1, they have identical molar loadings with the Ni_1Re_1 catalyst. For comparison, Ni_1Mo_1 and Ni_1Fe_1 catalysts with 10 wt% Ni loading relative to support were also prepared using above the method. Prior to use, the calcined samples were reduced at 500 °C for 3.0 h.

2.3. Catalyst characterization

Hydrogenation temperature programmed reduction (H_2-TPR) was employed to study the reducibility of catalysts. The dispersion of metal particles over the catalyst surface was observed and measured by transmission electron microscope (TEM). X-ray diffraction (XRD) and high resolution transmission electron microscope (HRTEM) were used to analyze the formed species on the catalysts. The electronic interaction between metals was explored by XPS and in situ FTIR spectroscopy of CO (CO-FTIR). The amounts of hydrogen adsorption and acidic sites were measured by hydrogenation (H_2-TPD) and ammonia temperature programmed desorption (NH_3-TPD), respectively. The interaction between the reactant and tested catalyst was studied by in situ FTIR spectroscopy of propionic acid (PA). The measured information about the test procedure can be found in Supporting Information.

2.4. Computational details

To understand why the Ni_1Re_1 bimetallic catalyst shows high catalytic activity for the hydrogenation of fatty acids at a low temperature, the density functional theory (DFT) calculations were performed using the Perdew-Burke-Ernzerbof (PBE) approximation and the projector augmented wave (PAW) method in the Vienna Ab initio Simulation Package (VASP) [27]. 2 × 2 × 1 Monkhorst-Pack grid and an energy cutoff of 550 eV were used in our calculations [18]. The propionic acid (PA) was selected as a simplified model of fatty acids. A four-layer slab with 64 atoms for Ni(111) was modeled, a slab with 52 atoms for Re (111) and a larger slab with 144 atoms for Re_3Ni(111) was used. The vacuum length was set as 15 Å along the z direction. The upper two-layer atoms for all models in the cell were relaxed. The adsorption energy (E_{ads}) was calculated using the following equation [28]:

$$E_{ads} = E_{total} - E_{surface} - E_{adsorbate} \quad (1)$$

where E_{total} was the total energy after the adsorption, $E_{surface}$ was the calculated energy of the clean catalyst and $E_{adsorbate}$ was the energy of the gas-phase molecule.

2.5. Catalytic reaction and product analysis

The catalytic hydrogenation reaction was carried out in an autoclave reactor (50 mL). Typically, the reactor was added into fatty acid (0.1 g), activated catalyst (0.02 g) and cyclohexane solvent (10 mL). Then, the reactor was pressurized with hydrogen to 4.0 MPa after removing air inside. The reactions were operated at a temperature range of 130–170 °C under a stirring rate of 1000 rpm. After the reaction, the obtained liquid product was analyzed by gas chromatography (GC, Agilent 7890 A/5975 C) equipped with a FID and an (30 m × 0.25 mm × 0.25 μm) HP-5 capillary column. Internal standard (i.e., eicosane) was used for quantitative analysis.

The conversions of substrates and selectivity of target product were calculated using the following Eqs. (2–3):

$$\text{Conversion} = \frac{\text{mol}_{\text{initial reactant}} - \text{mol}_{\text{unreacted reactant}}}{\text{mol}_{\text{initial reactant}}} \times 100\% \quad (2)$$

$$\text{Selec. (detec. products)} = \frac{\text{mol}_{\text{product}} \times \text{n}_{\text{C atoms in product}}}{\text{mol}_{\text{total C atoms in the liquid products detected}}} \times 100\% \quad (3)$$

3. Results and discussion

3.1. Catalyst characterization

The textural properties of the Ni_xRe_y/SBA-15 catalysts with different molar ratio of Ni/Re were analyzed by using N_2 adsorption-desorption, XRD, CO pulse adsorption, H_2-TPR and TEM. The N_2 adsorption-desorption isotherms of the catalysts were displayed in Fig. S1 (a). All tested catalysts exhibited typical type VI isotherms with evident H1 hysteresis loop, indicating that the tested catalysts were typical mesoporous structure. Fig. S1 (b) shows the corresponding pore size distribution curves and revealed that the pore sizes were centered at about 6–8 nm. The detailed textural parameters are listed in Table S2. Compared with the SBA-15 support without any metal loadings, the surface areas and total pore volume of the Ni_xRe_y/SBA-15 catalysts gradually decreased as the metal loading increased. In particular, when the Ni/Re < 1 ($Ni_1Re_{1.5}$ and Ni_1Re_2), the surface area of the catalyst was drastically reduced, which could be attributed to the excessive Re metal loadings to form large metal particles, as indicated by the XRD results.

XRD was performed to identify the phase composition of the catalysts. As shown in Fig. 1(a), after reduction at 500 °C for 3.0 h, the monometallic Ni_1 and Re_1 catalysts only showed the metallic Ni and Re diffraction peaks, respectively, while the Ni_xRe_y bimetallic catalysts with different molar ratio exhibited a different behavior from the Ni_1 and Re_1 catalysts. In the bimetallic Ni_xRe_y catalysts, for which the introduction of Re component resulted in the lattice expansion of Ni unite cell, the diffraction peak of Ni (111) at 2θ of 44.3° for monometallic Ni_1 shifted to a lower value of 43.7 ° for the Ni_1Re_1 catalyst. This phenomenon reveals that the introduced Re component penetrated into the Ni lattice and formed NiRe alloy. Moreover, no Ni species were detected in the bimetallic Ni_xRe_y catalysts, indicating that the presence of Re favored the dispersion of Ni species. With the introduction of Re component, it was observed that the $Ni_1Re_{1.5}$ and Ni_1Re_2 catalysts displayed the diffraction peaks of metallic Re, which results from the reduction of excess Re species to form large metal particles.

H_2-TPR was conducted to investigate the reducibility of catalysts and the interaction between metals (Fig. 1(b)). The Ni_1 and Re_1 only exhibited one hydrogen reduction peak at around 405 (Ni^{2+} to Ni^0) [29] and 288 °C (Re^{n+} to Re^0) [30], respectively. As for the Ni_xRe_y bimetallic catalysts, interestingly, it was found that they also only showed one reduction peak at around 305 °C, in which the peak position was located between Ni_1 and Re_1. This result suggests that the presence of Re promoted the reduction of NiO (shifted from 405 to 305 °C) due to their strong interaction. Additionally, only one large hydrogen reduction peak appeared in the bimetallic catalysts indicates that the introduced Ni and Re species may form another compound of NiRe alloy during catalyst reduction process, as implied in the characterization results of XRD and HRTEM (Fig. 2(c′)).

In order to observe the dispersion of metal particles on the catalyst surface, TEM images were made. As shown in Fig. 2(a, b), the nickel particles on the surface of Ni_1 catalyst were obviously agglomerated, while the Re_1 catalyst exhibited the uniform and small metal particles with average particle sizes of 6.2 nm. These results indicate that Re species can be better dispersed on the SBA-15 support as compared with the Ni species, which could be attributed to the strong oxophilicity of Re species [31]. As for the Ni_1Re_1 catalysts, it was found that the introduction of Re significantly reduced the metal particles with the average size of 5.6 nm (Fig. 2(c, d)), indicating that the added Re promoted the dispersion of Ni species, in accordance with the XRD results. To further confirm this phenomenon, CO pulse adsorption was performed to calculate the dispersion of metallic Ni (Table S2). After introducing the Re species, the dispersion of metallic Ni was improved from 1.8% of the Ni_1 to 3.2% of the Ni_1Re_1 catalyst. According to the characteristic results (XRD, H_2-TPR, XPS and CO-FTIR), the promotional effect of Re on the dispersion of the metallic Ni was attributed to the interaction between the Ni and Re.

HRTEM measurements were performed to identify the formed species on the surface of support. For the Ni_1 and Re_1 catalysts, the lattice fringes of 0.204 and 0.21 nm were measured (Fig. 2(a′, b′)), corresponding to the Ni (111) and Re (101) spacings, respectively. As for the Ni_1Re_1 catalyst, the lattice fringe of 0.206 nm was measured (Fig. 2(c′)), which was ascribed to the NiRe alloy [31]. In good agreement with the XRD and H_2-TPR results, these confirm the formation of NiRe alloy. Additionally, elemental mapping and line scanning of Ni_1Re_1 were also performed (Fig. 2(e, f)). The result of mapping analysis showed that the Ni and Re species were successfully dispersed on the SBA-15 surface. A similar trend of Ni and Re components displayed in the line scanning profile indicated that Ni and Re species existed an interaction.

XPS was used to analyze the oxidation state of catalysts and the

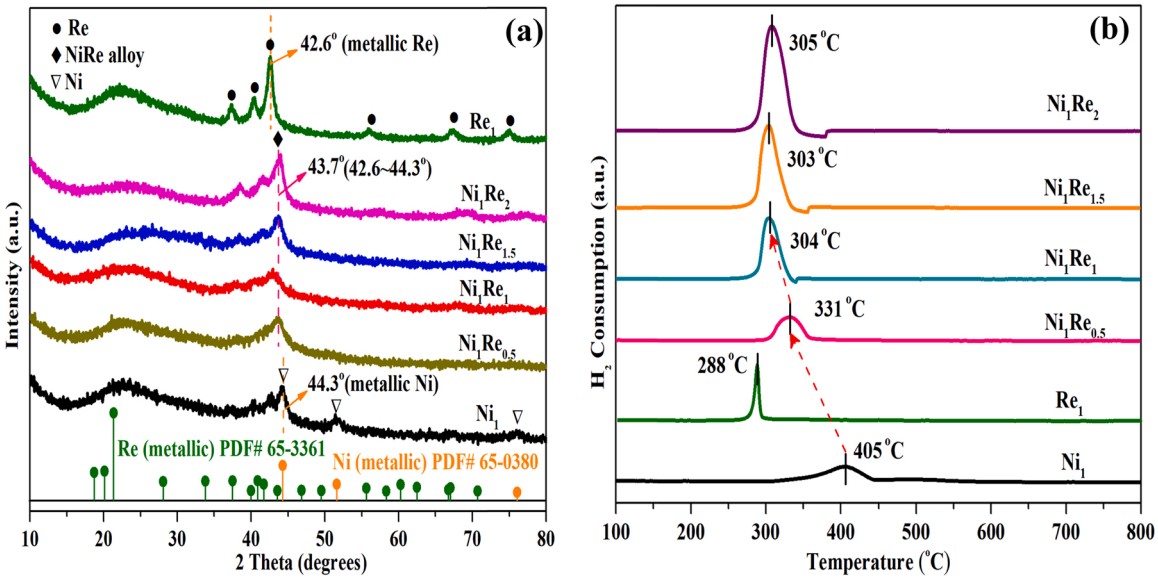

Fig. 1. (a) XRD patterns of the reduced catalysts; (b) H_2-TPR profiles of the calcined catalysts.

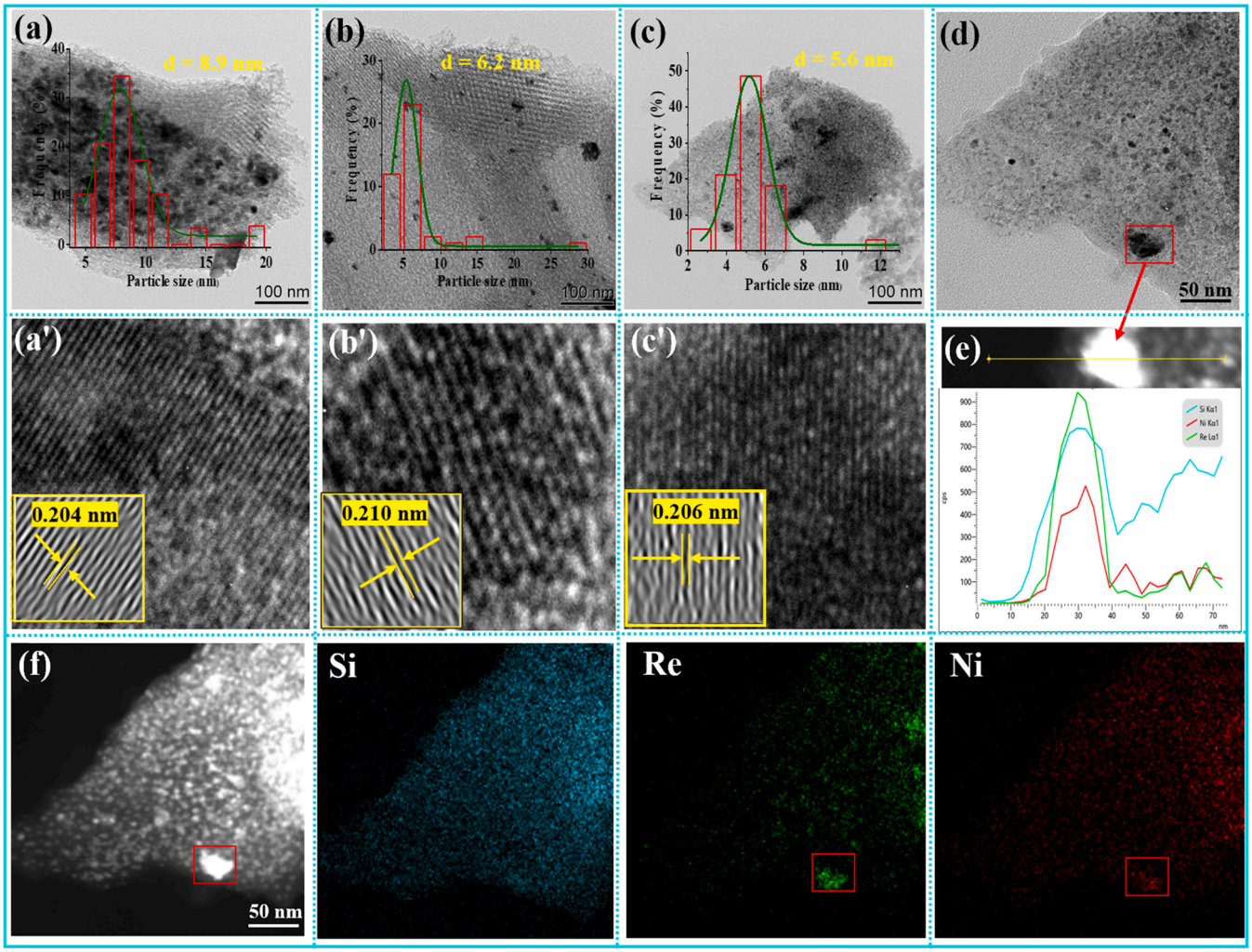

Fig. 2. TEM images of (a) Ni_1; (b) Re_1; (c and d) Ni_1Re_1; HRTEM image of (a′) Ni_1; (b′) Re_1; (c′) Ni_1Re_1; (e) EDS line spectra along the yellow line in e image; (f) HADDF-STEM image and elemental mapping of Ni_1Re_1 catalyst.

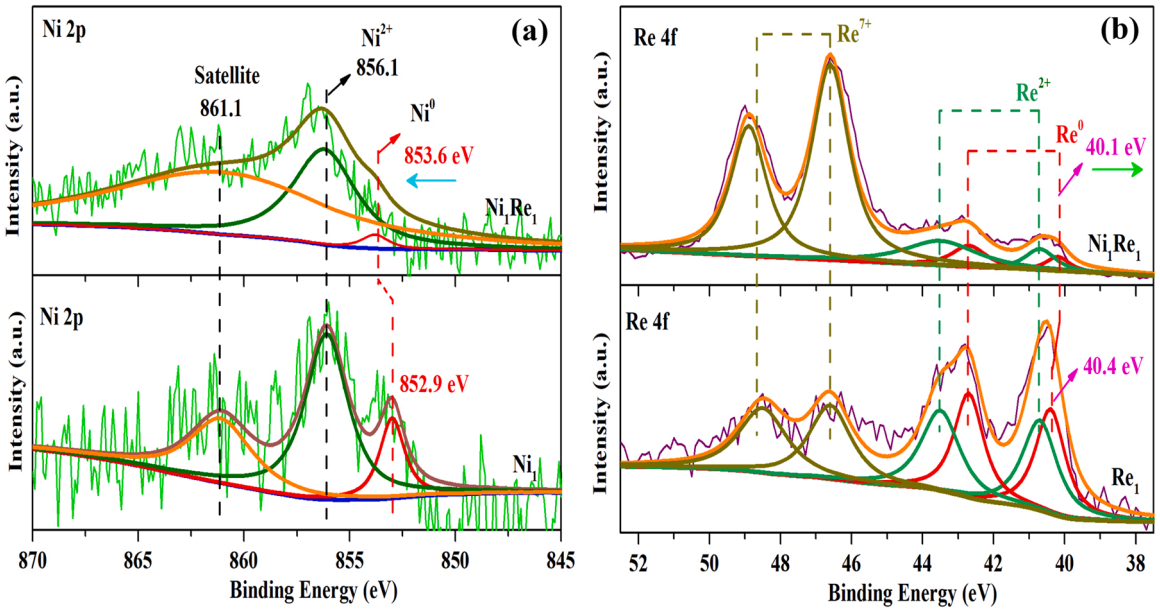

Fig. 3. XPS spectra of (a) Ni 2p and (b) Re 4 f for the reduced catalysts.

possible electronic interaction between metals. Fig. 3(a) shows the Ni 2p spectra and corresponding divided peaks of each sample. For the monometallic Ni_1 catalyst, the Ni 2p spectra displayed three deconvoluted peaks, locating at 852.9, 856.1 and 861.1 eV, which were ascribed to the Ni^0, Ni^{2+} and its satellite peak [32], respectively. As compared with the Ni_1 catalyst appeared at 852.9 eV for Ni^0, the binding energy (BE) of Ni^0 shifted to higher BE (+0.7) in the Ni_1Re_1 catalyst, indicating the electron transfer from the metallic Ni to Re. Fig. 3(b) shows the Re 4 f spectra of Re_1 and Ni_1Re_1 catalysts. Divided peaks of each sample showed a mixture of different oxidation states (Re^0, Re^{2+}, Re^{7+}) [21,33]. As expected, the characteristic peak of Re^0 in the Ni_1Re_1 catalyst shifted to lower BE (from 40.4 eV in Re_1 catalyst to 40.1 eV) as compared with the monometallic Re_1 catalyst. The increase in BE of metallic Ni and the decrease in BE of metallic Re in the Ni_1Re_1 catalyst suggest that there is an electronic interaction between Ni and Re species.

In order to further investigate the interaction between Ni and Re species, in situ FT-IR of CO adsorption-desorption on Ni_1 and Ni_1Re_1 catalysts were performed (Fig. 4). Typically, the band appeared in below 2000 cm^{-1} was attributed to the multi-coordinated adsorption of CO, while the band located in above 2000 cm^{-1} was ascribed to the linear adsorption of CO [34]. It was reported that CO was hardly adsorbed on the Re species (metallic Re and ReO_x) at room temperature [31], therefore, the bands shown in Fig. 4 were assigned to the CO adsorption on Ni atoms. From Fig. 4((a, b)), it was observed that the Ni_1Re_1 catalyst only showed the bands of linear adsorption of CO, while the Ni_1 catalyst exhibited both multi-coordinated adsorption (1628 cm^{-1}) and linear adsorption of CO. This may be due to the fact that introducing Re breaks the contiguous Ni atoms and forms much small Ni ensembles, which suppressed the multi-coordinated adsorption of CO on Ni atoms.

Besides, it was observed that the band of linear CO adsorption showed a blue-shift from 2040 cm^{-1} on Ni_1 to 2053 cm^{-1} on Ni_1Re_1. Combining the above XPS results, this shift may result from the electronic interaction between Ni and Re species, which the decrease of Ni electron density results in the weakening of Ni-C bonds and strengthening of C-O bonds [31], and thus leading to the bule-shift of $\nu(C{\equiv}O)$. Additionally, we can clearly see that, after flushed with flow N_2 for 20 min, Ni_1Re_1 catalyst still exhibited the strong adsorption peaks of CO, while the peaks were not detected on the Ni_1 catalyst. This suggests that Ni_1Re_1 bimetallic catalyst provided more active sites for the CO linear adsorption, and these sites have strong interaction with CO. Carbon monoxide as a simplified model for C═O group, the strong interaction indicates that the reactant molecules containing C═O groups can be better adsorbed on the Ni_1Re_1 bimetallic catalyst.

Catalyst acidity plays an important role in promoting the conversion of fatty acids and improving the selectivity of fatty alcohols. Appropriate acid site concentrations are beneficial for the reaction, while the weak and strong acid concentrations usually result in the low catalytic activity and the occurrence of side reactions like C-C bond cleavage, respectively. To study the influence of the introduced Re species on the catalyst acidity, NH_3-TPD characterization was performed. According to the different NH_3 desorption temperatures, the acidic sites were divided into three types of weak (T < 300 ℃), medium (300 ℃ < T < 450 ℃) and strong acid sites (T > 450 ℃) [35]. As shown in Fig. 5(a), all tested catalysts were dominated by weak and medium acid sites. As compared with the monometallic Ni_1 catalyst, introducing Re species greatly increased the number of weak and medium acid sites. This could be attributed to the unsaturated Re^{n+} species, as proved in the XPS characterization. The corresponding acid concentrations were obtained based on the fitted peak area (Fig. 5(b)). With the introduction of Re species, the total acid concentration was gradually increased. However, when excessive Re species were added, it was noted that a large number of strong acid sites were detected on the $Ni_1Re_{1.5}$ and Ni_1Re_2 catalysts (Fig. 5(a)). Based on the XRD characteristic results, this may be caused by excessive Re species forming large metal particles. These results suggest that the acidity of Ni_xRe_y catalysts mainly result from the introduction of the Re species, however, adding an excessive amount of Re species would result in the appearance of strong acid sites.

3.2. Catalytic performance towards hydrogenation of fatty acids

In order to evaluate the catalytic performance in the hydrogenation of fatty acids, all synthesized catalysts were applied to hydrogenation of stearic acid. As shown in Fig. 6(a), at a low temperature of 150 °C, monometallic Ni_1 and Re_1 catalysts exhibited low catalytic activities with conversion rates of < 10%. In contrast, the Ni_xRe_y bimetallic catalysts with different molar ratio showed remarkably enhanced catalytic performance, where the main products were stearyl alcohol and a small amount of side product of alkanes. The optimum catalytic performance

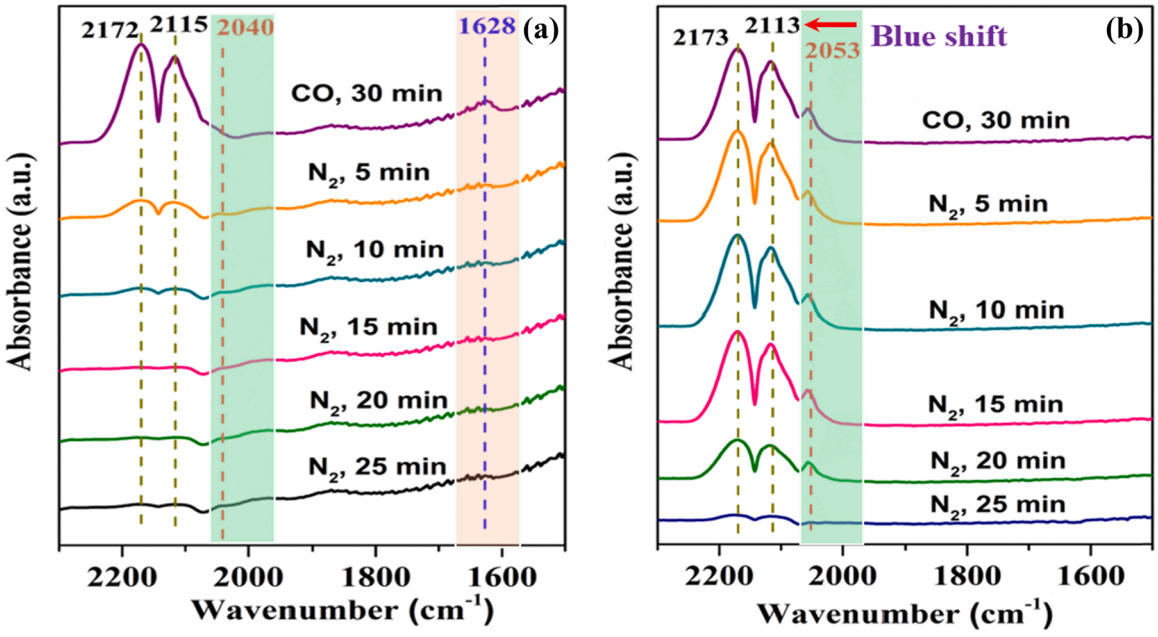

Fig. 4. In situ FTIR of CO adsorption over the reduced catalysts at room temperature for 30 min in a CO flow, and then desorption in N_2 flow for 5, 10, 15, 20, 25 min of (a) Ni_1 and (b) Ni_1Re_1.

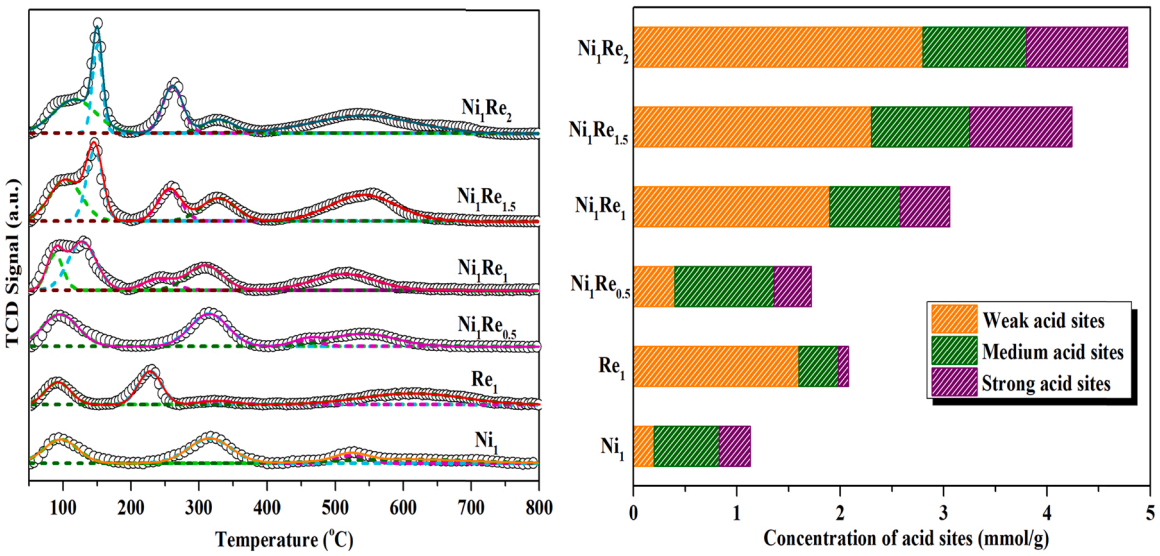

Fig. 5. (a) NH_3-TPD profiles of the reduced catalysts; (b) corresponding acid concentration obtained by calculating the fitted peak area.

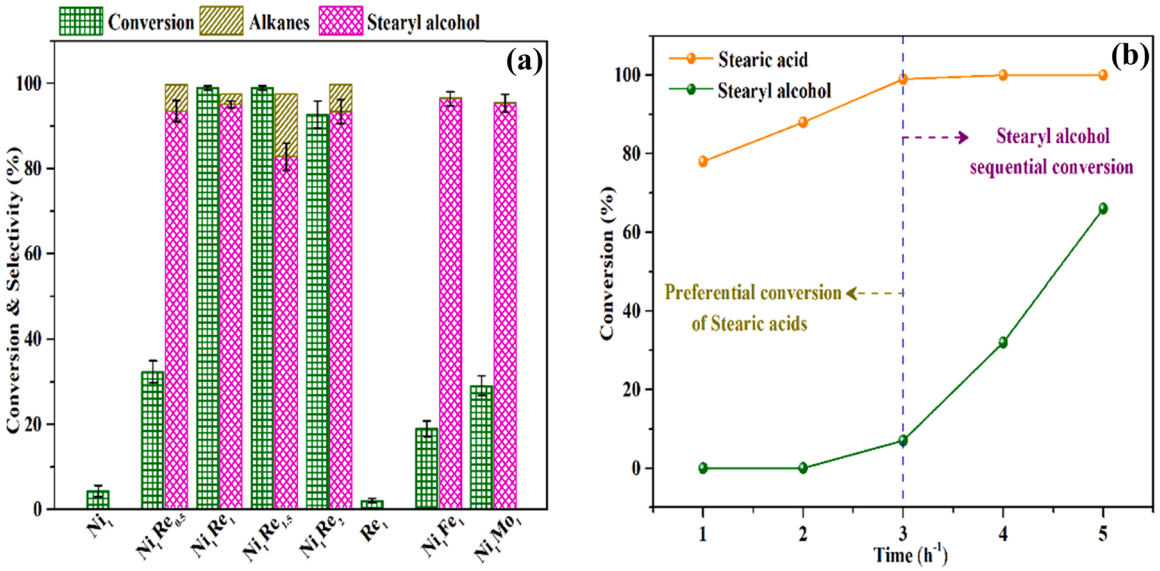

Fig. 6. (a) the conversion of stearic acid and product distributions over the different catalysts; (b) competitive conversion of stearic acid and stearyl alcohol over the Ni_1Re_1 catalyst with reaction time. Reaction conditions: (a) 0.1 g stearic acid, 0.02 g catalyst in 10 mL cyclohexane at 150 °C and 4.0 MPa H_2 for 5 h, (b) reactants containing both stearic acid (0.05 g) and stearyl alcohol (0.05 g), other reaction parameters are the same as (a).

was observed on the Ni_1Re_1 catalyst with 100% conversion and 95% selectivity towards stearyl alcohol. Further increasing Re loading (Ni_1Re_2 catalyst) resulted in the decrease of catalyst activity and selectivity. Decreasing surface area, large Re metal particles and strong acid sites on the Ni_1Re_2 catalysts may be the main reason for the decrease of catalytic performance, as indicated by the above XRD (Fig. 1(a)) and NH_3-TPD (Fig. 5) characterizations. On the other hand, it was reported that the FeO_x- [18] and MoO_x-modified [36,37] metallic Ni catalysts are efficient for hydrogenation of fatty acids/esters. For comparison, their catalytic activities were tested under the selected conditions and found to be ineffective. These results suggest that introducing Re component is essential to realize the low-temperature hydro-conversion of stearic acid. According to the above catalyst characterization, it is known that there is an interaction between Ni and Re species in the bimetallic catalysts, therefore, we infer that the interaction may be responsible for its high catalytic activity. To verify this speculation, a physical mixture of Ni_1 and Re_1 was tested and showed similar stearic acid conversion (6.5%) as the Ni_1 catalyst, indicating the importance of a combination of a proximate Ni and Re species.

Next, we used stearic acid and stearyl alcohol as raw materials to study their conversion process on the Ni_1Re_1 catalyst (Fig. 6(b)). At the beginning of reaction (0–3 h), stearic acid was first converted, while stearyl alcohol was not consumed at the presence of stearic acid. After 3 h reaction, stearyl alcohol begin to be converted when stearic acid was completely consumed. This result suggests that stearic acid was preferentially adsorbed and converted on the Ni_1Re_1 catalyst than the stearyl alcohol. In other words, the presence of stearic acid can inhibit the conversion of stearyl alcohol on the Ni_1Re_1 catalyst. This is consistent with prior study of fatty acid over the ReO_x-Pd/SiO_2 catalyst [38]. The preferential conversion sequence of fatty acids and fatty alcohols on the Ni_1Re_1 catalyst makes it possible to selectively obtain fatty alcohols and diesel-range alkanes with high yields by adjusting reaction temperature. This feature of the Ni_1Re_1 catalyst may be attributed to its strong electrophilicity, as indicated in the CO-FTIR characterization (Fig. 4). Since

the carbonyl oxygen of fatty acids is more electronegative than the hydroxyl oxygen of fatty alcohols [39], thus, the fatty acids are preferentially adsorpted and converted on the catalyst surface than the fatty alcohols.

Fig. 7(a) shows the time-course experiments of stearic acid, and reveals that the reactant was gradually converted to products with time. In the initial reaction stage of 2 h, the products were stearyl alcohol and a small amount of alkanes and stearyl stearate. After 5 h reaction, the reactant was completely converted and the dominant product was stearyl alcohol. Further prolonging the reaction time (6 h), the obtained fatty alcohol was gradually converted into alkanes containing C_{17} and C_{18} alkanes via dehydrogenation-decarbonylation route (DCO route) and dehydration-hydrogenation route (HDO route), respectively, as shown in Scheme 1. The optimum reaction time was 5 h, in which the reactant was completely converted and the selectivity of fatty alcohol was the highest (95%). Fig. 7(b) shows the effect of reaction temperature on the conversion and product distributions. This result suggests that, by adjusting reaction temperature, fatty alcohols or alkanes with high yields can be selectively obtained. For instance, fatty alcohols were the main product at a low temperature of 150 °C, while the alkanes were obtained at a higher temperature of 170 °C. In addition, by studying the influence of H_2 pressure on the hydrogenation reaction, it was found that 4.0 MPa H_2 pressure was satisfactory (Fig. S2).

Under the optimized reaction conditions, the scope of substrates was extended to other fatty acids such as octanoic acid, lauric acid, palmitic acid and oleic acid. As shown in Fig. 7(c), the Ni_1Re_1 bimetallic catalyst basically achieved quantitative saturated acids (octanoic acid, lauric acid and palmitic acid) conversion and gave their corresponding fatty alcohol as the dominate product. For the unsaturated acid of oleic acid, the relatively low conversion rate (92%) may be attributed to its unsaturated C=C bond, which consumed a large amount of hydrogen molecules in reaction system. Further raising the reaction temperature to 170 °C, the diesel-range alkanes with high yields can be obtained. Table 1 displays the performance of Ni_1Re_1 catalyst and a comparison with previous reported catalyst system during the hydrogenation of fatty acids [11,16,18,40–44]. The developed Ni_1Re_1 catalyst shows excellent

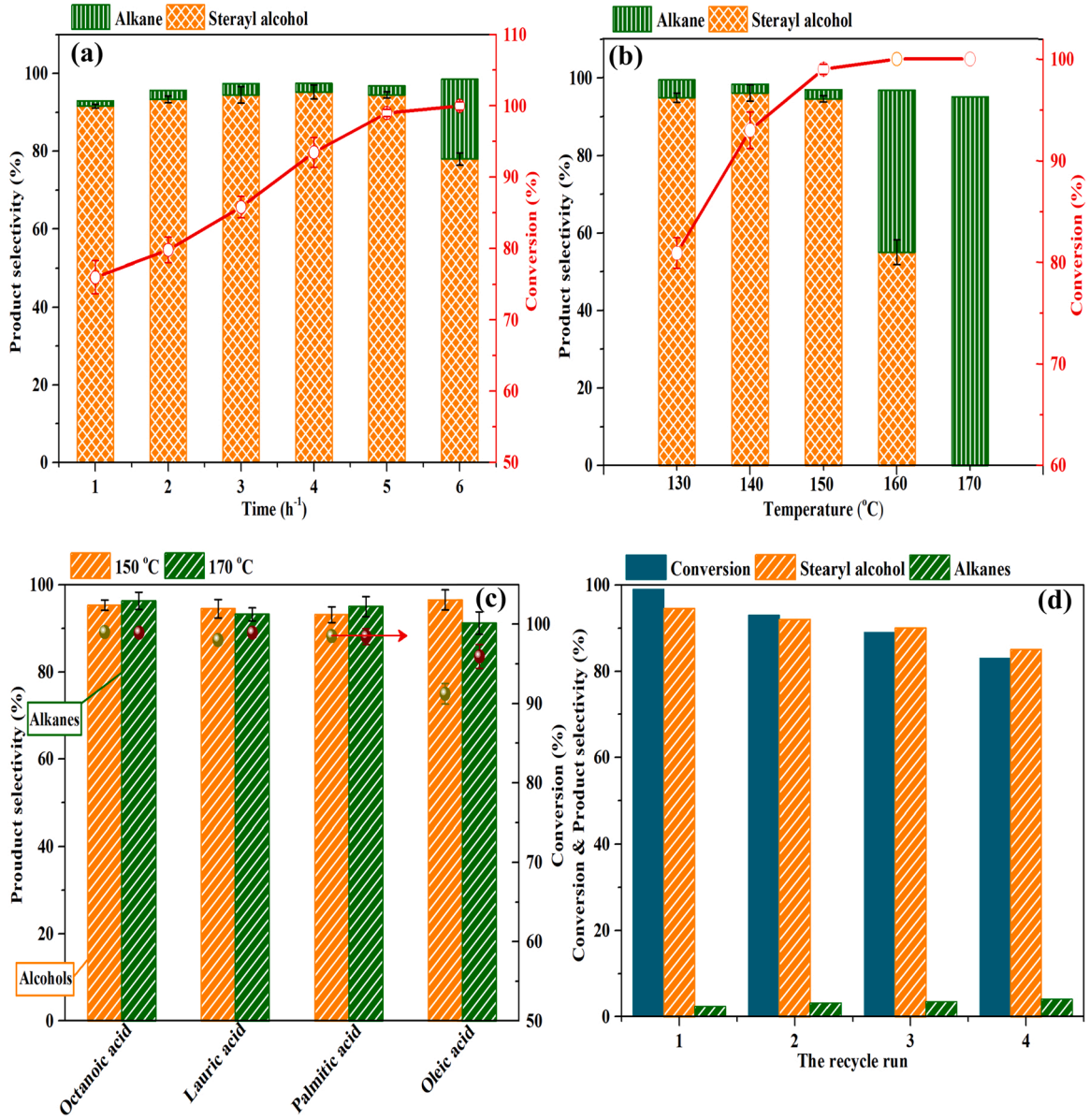

Fig. 7. Catalytic conversion and the main product distributions as function of (a) reaction time, (b) reaction temperature, (c) hydrogenation of various fatty acids and (d) catalyst recycling test on the Ni_1Re_1 catalyst. General conditions: (a) 0.1 g stearic acid, 0.02 g catalyst (Ni_1Re_1 catalyst) in 10 mL cyclohexane at 150 °C and 4.0 MPa H_2 for 5 h.

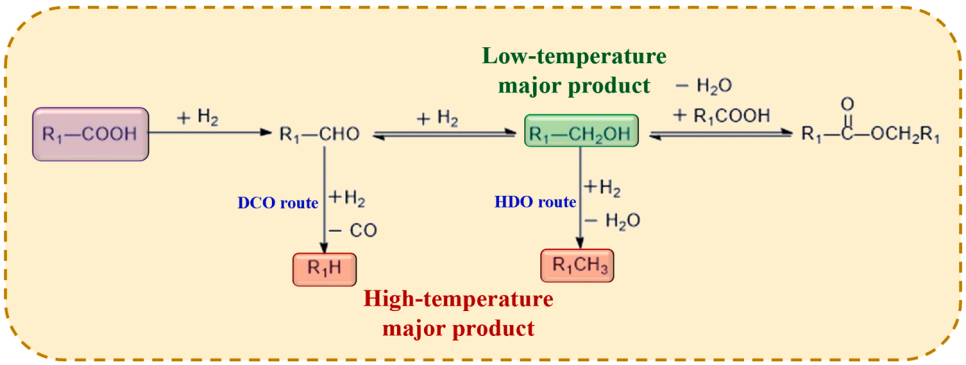

Scheme 1. Possible reaction pathway of fatty acids over the Ni_1Re_1 catalyst.

Table 1
The performance of Ni_1Re_1 in this work and comparison with previous reported studies.

Catalyst	Reaction conditions	Solvent	Conv. (%)	Alcohol selec. (%)	Alkane selec. (%)	Ref.
Ru-Sn/SiO_2	240 °C, 4.0 MPa	dodecane	100	99.0	0.55	40
Ru/NH_2-rGO	210 °C, 10.0 MPa	1,4-dioxane	> 99	93.0	—	41
Ni-Fe/C	250 °C, 5.0 MPa	1,4-dioxane	> 99	98.0	—	18
Ni-In/SiO_2	270 °C, 3.5 MPa	cyclohexane	100	94.1	—	16
Ni_1Re_1	150 °C, 4.0 MPa	cyclohexane	99	94.5	2.3	This work
Ir-ReO_x/SiO_2	180 °C, 2.0 MPa	cyclohexane	100	—	100%	11
Ru/HPA	180 °C, 2.0 MPa	H_2O	95.8	15	80.7	42
Ni/ZrO_2	260 °C, 3.0 MPa	dodecane	100	1.2	97.5	43
CuCo/CNT	260 °C, 3.0 MPa	decane	100	—	95.0	44
Ni_1Re_1	170 °C, 4.0 MPa	cyclohexane	100	—	95.0	This work

catalytic performance for production of diesel-range alkanes and fatty alcohols from the conversion of fatty acid at low temperature, and even better than noble metal catalysts. In addition, it is highlighted that, compared with the other catalysts, Ni_1Re_1 catalyst exhibits tunable selectivity towards alcohols and alkanes in a low-temperature range of 150 and 170 °C. These results are important not only for the conversion of waste cooking oils rich in fatty acids under mild conditions, but also for the selective hydrogenation of other biomass-derived compounds containing C═O/C-O and O-H groups.

Catalyst stability as an important indicator for evaluating heterogeneous catalyst was also studied (Fig. 7(d)). After the fourth recycling test, the conversion and selectivity towards stearyl alcohol were decreased by about 15% (from 99% to 84%) and 10% (from 95% to 85%), respectively. TEM, XPS and ICP-MS characterizations were employed to elucidate the decrease of the catalytic performance. TEM images (Fig. S3) showed that the metal nanoparticles after recycling were still evenly dispersed on the catalyst surface, and no obvious agglomeration was observed. The XPS spectra (Fig. S4) revealed that after recycles, the ratio of Ni^0 decreased from 9.2% to 4.3%, while the Re^0 decreased from 7% to 3.2%. ICP-MS results (Table S3) indicated that the contents of Ni (from 6.8 wt% to 6.3 wt%) and Re (from 21.8 wt% to 19.2 wt%) species were decreased after recycles. Therefore, the changes of catalyst activity and selectivity may be attributed to the oxidation of partially metal active sites and the leaching of metal elements. The

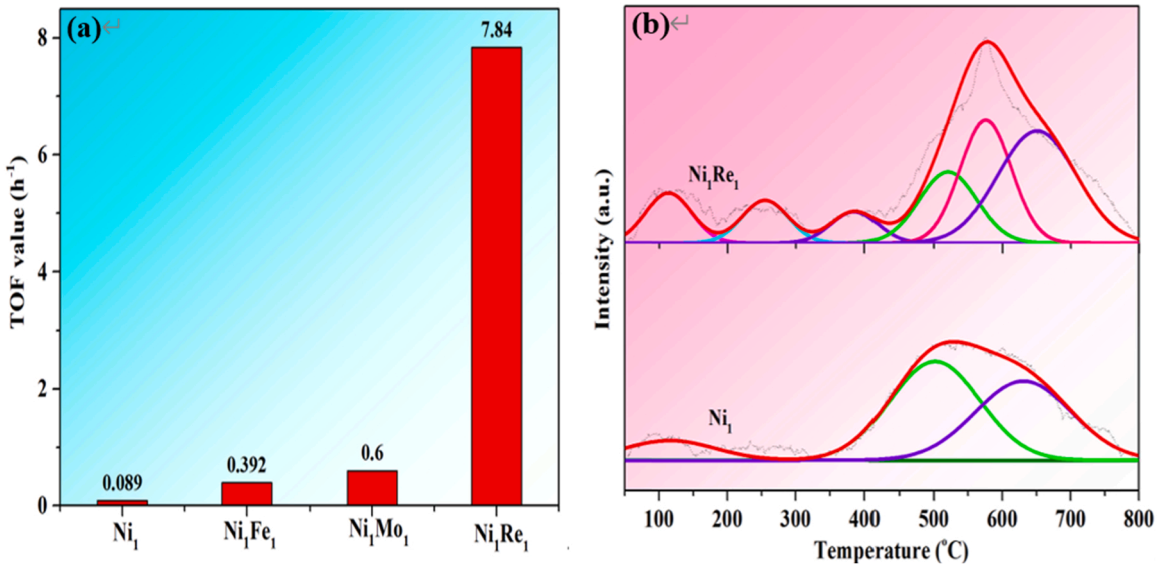

Fig. 8. (a) Comparison of TOF values over the different reduced catalysts. (b) H_2-TPD profiles of the reduced Ni_1 and Ni_1Re_1 catalysts.

above recycle results indicate that the reusability of the catalyst need to be further improved. In future work, how to inhibit the leaching of metal active species during reactions will be the focus of our research.

3.3. Studies on structure-activity correlation

Normally, bimetallic catalysts had higher catalytic performance due to their unique synergistic effects as compared with the monometallic catalysts in the HDO reactions. As shown in Fig. 8(a), bimetallic catalysts such as Ni_1Fe_1, Ni_1Mo_1 and Ni_1Re_1 showed higher TOF values than that of monometallic Ni catalyst under the identical reaction conditions. Among these bimetallic catalysts, Ni_1Re_1 catalyst exhibited highest TOF value, indicating that the introduction of Re species is crucial to enhance the catalytic activity. Based on the above characteristic results (XRD, HRTEM, XPS and CO-FTIR), it was known that the introduced Ni and Re species interacted with each other and were mainly dispersed on the surface of the catalyst in the form of NiRe alloy. Therefore, we infer that the high catalytic activity may be associated with the NiRe alloy, that is, promoting the dissociation/activation of H_2 and the adsorption/conversion of reactants at low temperatures.

In order to investigate the ability of H_2 dissociation/activition on the catalysts, H_2-TPD experiments were performed (Fig. 8(b)). Compared with the reference sample of Ni_1 catalyst showing the H_2 desorption peaks at high temperatures, several desorption peaks at a low temperature range (100–400 °C) were observed in the Ni_1Re_1 bimetallic catalyst. Moreover, the Ni_1Re_1 bimetallic catalyst showed a larger integral peak area than that of Ni_1 catalyst. These results indicate that introducing Re species can enhance hydrogen activation/dissociation ability, which can provide more active hydrogen atoms for the hydrogenation reaction. This enhanced H_2 activation/dissociation ability on the Ni_1Re_1 catalyst can also be supported by the following DFT calculation (Fig. 10).

To acquire more adsorbed information about the reactant on the catalysts, in situ FTIR of octanoic acid was conducted. As shown in Fig. 9 (A), a peak at 1720 cm^{-1} was detected corresponding to the carbonyl group (C═O) of the pure octanoic acid [45,46]. As the temperature increased from 25 °C to 150 °C, the peak gradually shifted to a higher wavenumber (1781 cm^{-1}), indicating that the ocatnoic acid was chemical adsorbed on the tested catalysts. Compared with the Ni_1 catalyst that showing a weak peak intensity at 1781 cm^{-1}, Ni_1Re_1 catalyst showed a strong peak intensity, expecially at 150 °C, where the adsorbed peak at 1721 cm^{-1} was completely shifted to 1781 cm^{-1}. This result demonstrates that, with an increased in reaction temperature, fatty acid molecules can be more stably adsorbed on the Ni_1Re_1 catalyst via interacting with carbonyl group of fatty acids when compared with the Ni_1 catalyst, and this interaction reached the strongest at 150 °C. Furthermore, to study the effect of introducing Re species on the reactant adsorption, in situ FTIR spectrum of the octanoic acid on the NiRe catalysts with various Ni/Re ratios were carried out. As shown in Fig. S5, monometallic Re_1 and bimetallic Ni_xRe_y catalysts exhibited a higher adsorption intensity as compared with the Ni_1 catalysts under the identical desorbed temperature, which suggests that the introduction of Re species enhanced the interaction between the reactant and catalyst, in accordance with the DFT calculation results.

On the other hand, the adsorbed information about the reactant on the Ni_1Fe_1 and Ni_1Mo_1 catalysts was also investigated for comparison. It was observed that the Ni_1Fe_1 and Ni_1Mo_1 catalysts showed stronger peak intensity at 1781 cm^{-1} under the identical adsorbed temperatures as compared with the Ni_1 catalyst. This indicates that introducing the second metal (Fe and Mo) is beneficial to promote the adsorption of fatty

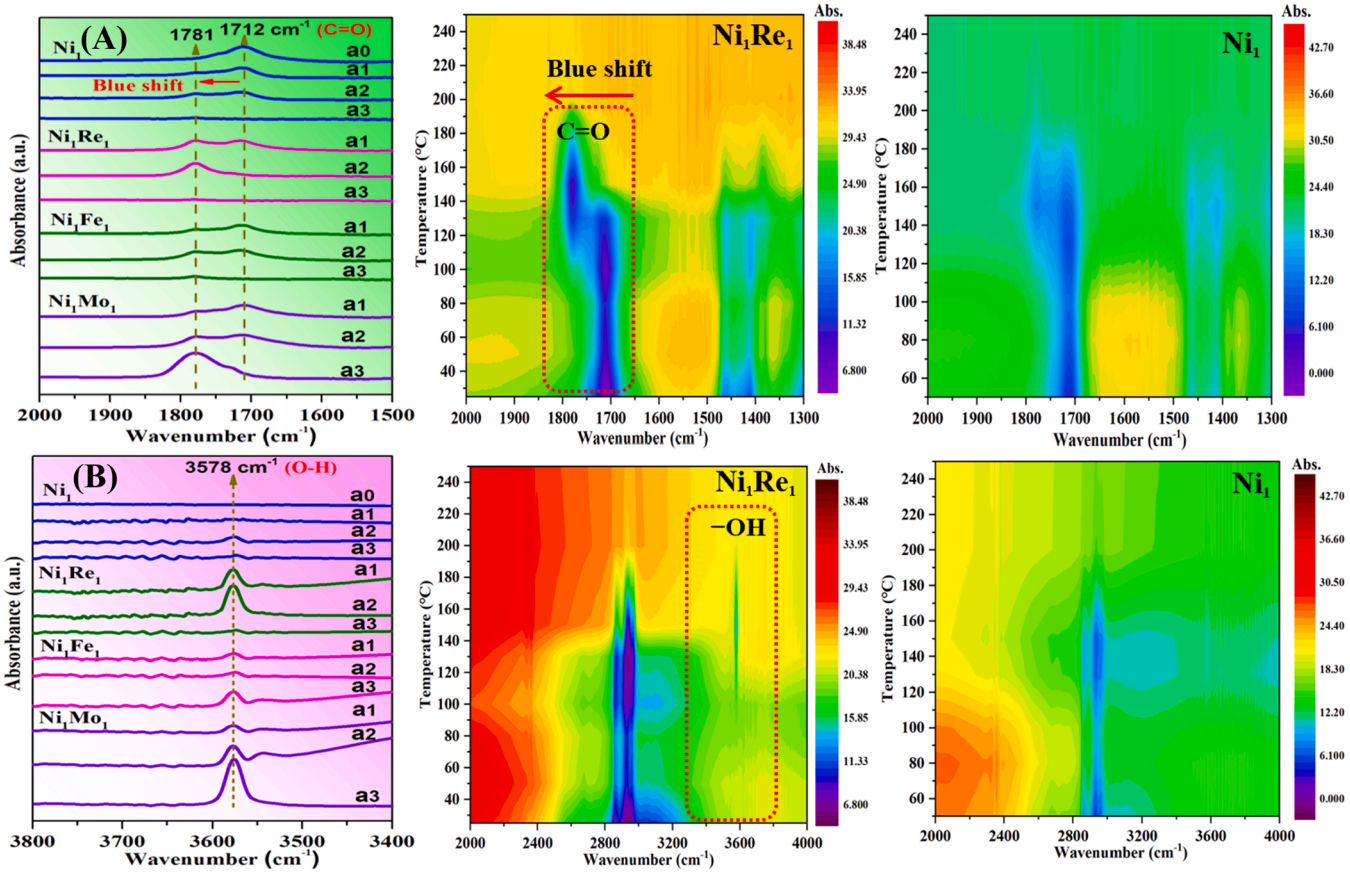

Fig. 9. In situ FTIR spectra of octanoic acid at 1500–2000 cm^{-1} (A), 3400–3800 cm^{-1} (B) over the Ni_1, Ni_1Re_1, Ni_1Fe_1 and Ni_1Mo_1 catalysts: (a0) 25 °C, (a1) 130 °C, (a2) 150 °C, (a3) 200 °C.

acids due to their higher oxophilicity than the metallic Ni. Secondly, analyzing the spectra of the bimetallic catalysts found that the temperatures of Ni_1Re_1, Ni_1Fe_1 and Ni_1Mo_1 catalysts achieving completely transformation from 1712 to 1781 cm^{-1} were 150, 200 and 200 °C, respectively. This reveals that, compared with the Ni_1Fe_1 and Ni_1Mo_1 catalysts, Ni_1Re_1 catalyst can chemically adsorb the fatty acids at a lower temperatures (150 °C) via interacting with carbonyl group.

Another difference in the spectra for these catalysts was the band at 3578 cm^{-1}, which is attributed to the hydroxy group of fatty alcohol products [42]. As shown in Fig. 9(B), Ni_1 catalyst showed a weak peak intensity, while Ni_1Re_1, Ni_1Fe_1 and Ni_1Mo_1 bimetallic catalysts showed a strong peak intensity. As the environmental temperature increased, the peak intensity gradually becomes stronger. Moreover, it is noted that as the peak intensity of the carbonyl group (C═O) of the octanoic acid decreased (Fig. 9(A)), the intensity of the hydroxy group gradually increased, indicating that the octanoic acid are gradually transformed to octanol as temperature increased. Among these bimetallic catalysts, Ni_1Re_1 and Ni_1Mo_1 catalysts showed higher peak intensity than that of Ni_1Fe_1 catalyst. Compared with the Ni_1Mo_1 catalyst that showing strong peak intenstiy at 200 °C, Ni_1Re_1 catalyst exhibited the highest peak intensity at 150 °C. These results proved that Ni_1Re_1 catalyst can adsorbe and convert fatty acid molecules into fatty alcohols at a lower temperature as compared with the Ni_1, Ni_1Fe_1 and Ni_1Mo_1 catalysts, in accordance with the experimental results shown in Fig. 6(a).

In order to further study the ability of H_2 dissociation/activition and the adsorption behavior of fatty acids on the metallic Ni, Re, and NiRe alloy, DFT calculations are carried out (Fig. 10). The Ni (111), Re (111) and Re_3Ni alloy (111) catalysts were constructed as simplified models for calculations in this work. Here, a more negative adsorption energy value represents a stronger interaction and a more stable adsorption state [39]. For the hydrogenation reaction, it is known that the H_2 dissociation/activition on the surface of catalyst is usually a prerequisite.

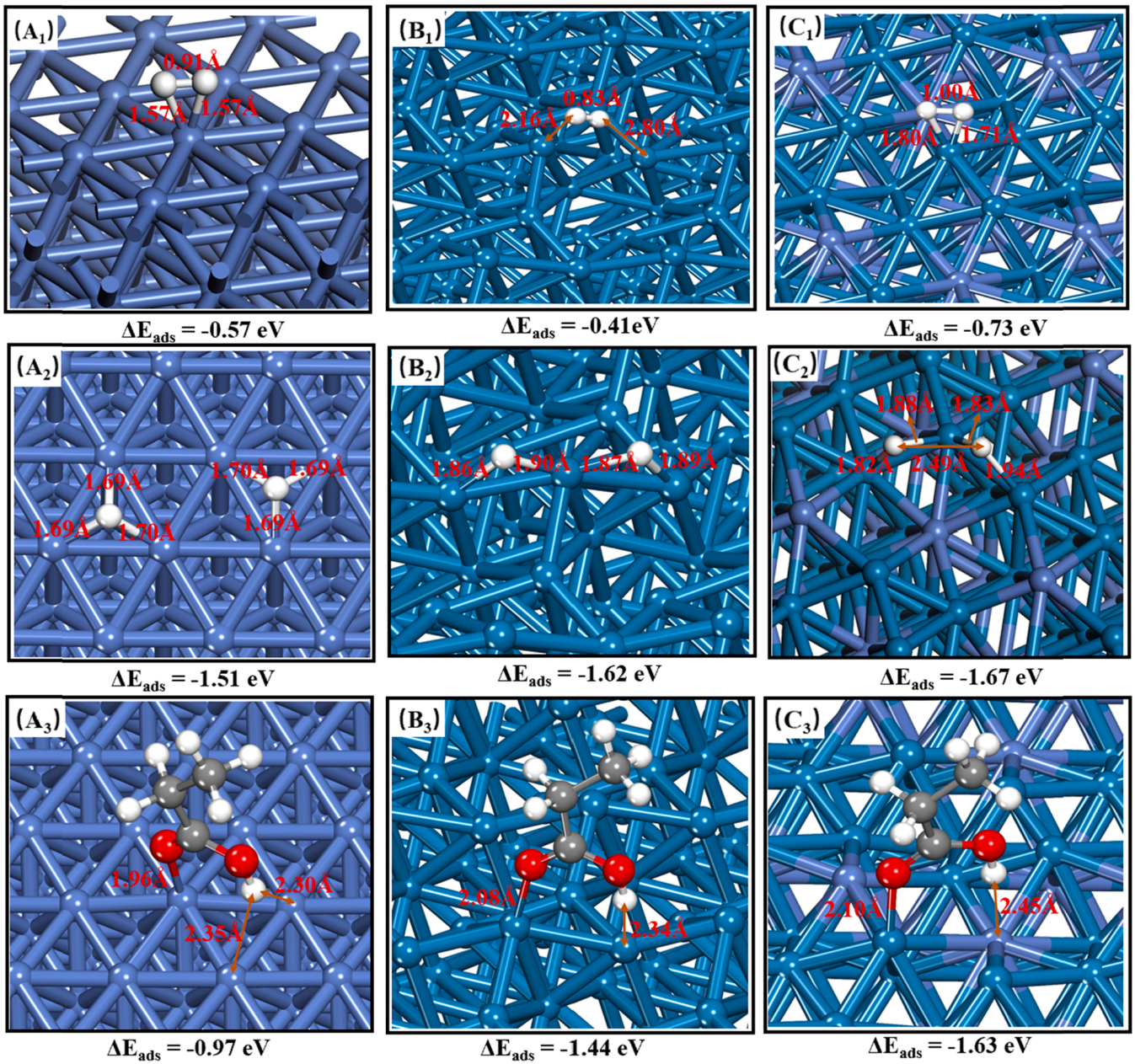

Fig. 10. Optimized adsorption structures of H_2 on (A_1) Ni (111), (B_1) Re (111) and (C_1) Re_3Ni alloy (111); of H * on (A_2) Ni (111), (B_2) Re (111) and (C_2) Re_3Ni alloy (111); of PA molecular on (A_3) Ni (111), (B_3) Re (111) and (C_3) Re_3Ni alloy (111). Ni: purple; Re: dark green; O: red (in PA); H: white; C: dark gray.

Therefore, we first studied the ability of H_2 dissociation/activition on the above-mentioned catalyst models. As shown in Figure 10A_1-C_1, the Re_3Ni alloy (111) showed a stronger interaction with H_2 molecules as compared with the Ni (111) catalyst (adsorption energies: −0.73 vs −0.57 eV). This strong interaction between the Re_3Ni alloy (111) and H_2 molecules greatly promoted the dissociation of H_2 and thus provided more active hydrogen atoms for the hydrogenation reaction, as proved in Figure 10A_2-C_2.

Fig. 10 C_1-C_3 shows the adsorption state of propionic acid (PA: a model molecule of fatty acids) on the Ni (111), Re (111) and Re_3Ni alloy (111) models. The above three models reveals that the PA molecule was adsorbed on the surface of catalysts through the interaction with oxygen atom of carbonyl group of fatty acids, in consistent with the characteristic results of Fig. 9(A). The calculated results showed that the adsorption energies over the Ni (111), Re (111) and Re_3Ni alloy (111) were −0.97, −1.44 and −1.63 eV, respectively. The Re_3Ni alloy (111) showed the highest negative PA adsorption energy, suggesting that PA could be more stably adsorbed on the surface of Re_3Ni alloy (111) catalyst. These calculation results are in accordance with the above H_2-TPD and in-situ FTIR characterizaiton results. In summary, from the above characterizaiton and DFT calculation results, it can be concluded that the high catalytic performance of NiRe bimetallic catalysts was mainly attributed to its strong ability of H_2 dissociation/activition and strong oxophilicity for the adsorption of fatty acids at low temperature.

4. Conclusions

In summary, we reported an efficient and environmentally benign catalytic system for the hydrogenation of fatty acids under remarkably low temperatures over the Ni_1Re_1 catalyst. At 150 °C, a high fatty acids conversion (>95%) and fatty alcohols selectivity (> 90%) can be obtained. Further increasing the temperature to 170 °C, the reactant can be completely converted into diesel-range alkanes. Studies on structure-activity correlation indicate that the high catalytic activity was attributed to the formation of NiRe alloy, which improved the dispersion of metallic Ni, the ability of H_2 dissociation/activation, and enhanced the adsorption of fatty acids/alcohols. The high selectivity towards target products was ascribed to its strong electrophilicity, making fatty acids preferentially adsorb on the catalyst surface than fatty alcohols, which results in high efficiency and inhibits the conversion of target products during the reaction. These features of the Ni-Re bimetallic catalyst may also enable it applicable to the hydro-conversion of other biomass-derived oxygenates containing C═O/C–O and/or O–H groups into valuable chemicals and green biofuels.

CRediT authorship contributioion statement

Xincheng Cao: Validation, Formal analysis, Investigation, Writing – original draft. **Jiaping Zhao:** Methodology, Formal analysis. **Feng Long:** Conceptualization, Methodology. **Peng Liu**: Formal analysis. **Xia Jiang**: Validation. **Xiaolei Zhang:** Validation, Writing – review & editing, Formal analysis. **Junming Xu**: Conceptualization, Methodology, Formal analysis, Writing – review & editing. **Jianchun Jiang:** Conceptualization, Methodology, Writing – review & editing.

Declaration of Competing Interest

There are no conflicts of interest to declare.

Acknowledgements

The authors would like to thank the financial support provided by the National Natural Science Foundation of China (2019YFB1504005 and 2019YFB1504000).

Appendix A. Supporting information

Supplementary data associated with this article can be found in the online version at doi:10.1016/j.apcatb.2022.121437.

References

[1] L. Hermida, A.Z. Abdullah, A.R. Mohamed, Deoxygenation of fatty acid to produce diesel-like hydrocarbons: A review of process conditions, reaction kinetics and mechanism, Renew. Sustain. Energy Rev. 42 (2015) 1223–1233.
[2] X. Yao, T.J. Strathmann, Y. Li, L.E. Cronmiller, H. Ma, J. Zhang, Catalytic hydrothermal deoxygenation of lipids and fatty acids to diesel-like hydrocarbons: A review, Green. Chem. 23 (2021) 1114–1129.
[3] Y. Zhou, X. Liu, P. Yu, C. Hu, Temperature-tuned selectivity to alkanes or alcohol from ethyl palmitate deoxygenation over zirconia-supported cobalt catalyst, Fuel 278 (2020) 1–13.
[4] J. Pritchard, G.A. Filonenko, R. van Putten, E.J.M. Hensen, E.A. Pidko, Heterogeneous and homogeneous catalysis for the hydrogenation of carboxylic acid derivatives: History, advances and future directions, Chem. Soc. Rev. 44 (2015) 3808–3833.
[5] Z.H. Zhang, Q.W. Yang, H. Chen, K. Chen, X.Y. Lu, P.K. Ouyang, J. Fu, J.G. Chen, In situ hydrogenation and decarboxylation of oleic acid into heptadecane over a Cu-Ni alloy catalyst using methanol as a hydrogen carrier, Green. Chem. 20 (2018) 197–205.
[6] S. Brillouet, E. Baltag, S. Brunet, F. Richard, Deoxygenation of decanoic acid and its main intermediates over unpromoted and promoted sulfided catalysts, Appl. Catal. B: Environ. 148 (2014) 201–211.
[7] S.K. Kim, S. Brand, H.-S. Lee, Y. Kim, J. Kim, Production of renewable diesel by hydrotreatment of soybean oil: Effect of reaction parameters, Chem. Eng. J. 228 (2013) 114–123.
[8] H. Adkins, K. Folkers, The catalytic hydrogenation of esters to alcohols, J. Am. Chem. Soc. 53 (1931) 1095–1097.
[9] T. Turek, D.L. Trimm, N.W. Cant, The catalytic hydrogenolysis of esters to alcohols, Catal. Rev. 36 (1994) 645–683.
[10] Y.D. Zhou, L. Li, G.Y. Li, C.W. Hu, Insights into the influence of ZrO_2 crystal structures on methyl laurate hydrogenation over Co/ZrO_2 catalysts, ACS Catal. 11 (2021) 7099–7113.
[11] S. Liu, T. Simonetti, W. Zheng, B. Saha, Selective hydrodeoxygenation of vegetable oils and waste cooking oils to green diesel using a silica-supported Ir-ReO_x bimetallic catalyst, ChemSusChem 11 (2018) 1446–1454.
[12] A. Ali, B. Li, Y. Lu, C. Zhao, Highly selective and low-temperature hydrothermal conversion of natural oils to fatty alcohols, Green. Chem. 21 (2019) 3059–3064.
[13] H.G. Manyar, C. Paun, R. Pilus, D.W. Rooney, J.M. Thompson, C. Hardacre, Highly selective and efficient hydrogenation of carboxylic acids to alcohols using titania supported Pt catalysts, Chem. Commun. 46 (2010) 6279–6281.
[14] Z.Y. Pan, R.J. Wang, J.X. Chen, Deoxygenation of methyl laurate as a model compound on Ni-Zn alloy and intermetallic compound catalysts: Geometric and electronic effects of oxophilic Zn, Appl. Catal. B: Environ. 224 (2018) 88–100.
[15] Y. Zheng, N. Zhao, J.X. Chen, Enhanced direct deoxygenation of anisole to benzene on SiO_2-supported Ni-Ga alloy and intermetallic compound, Appl. Catal. B: Environ. 250 (2019) 280–291.
[16] L. Wang, X. Niu, J. Chen, SiO_2 supported Ni-In intermetallic compounds: Efficient for selective hydrogenation of fatty acid methyl esters to fatty alcohols, Appl. Catal. B: Environ. 278 (2020) 1–14.
[17] Z.H. Zhang, H. Chen, C.X. Wang, K.Q. Chen, X.Y. Lu, P.K. Ouyang, J.X. Chen, Efficient and stable Cu-Ni/ZrO_2 catalysts for in situ hydrogenation and deoxygenation of oleic acid into heptadecane using methanol as a hydrogen donor, Fuel 230 (2018) 211–217.
[18] X. Kong, Z. Fang, X. Bao, Z. Wang, S. Mao, Y. Wang, Efficient hydrogenation of stearic acid over carbon coated Ni-Fe catalyst, J. Catal. 367 (2018) 139–149.
[19] S. Liu, W. Zheng, J. Fu, K. Alexopoulos, B. Saha, D.G. Vlachos, Molybdenum oxide-modified iridium catalysts for selective production of renewable oils for jet and diesel fuels and lubricants, ACS Catal. 9 (2019) 7679–7689.
[20] S. Liu, S. Dutta, W. Zheng, N.S. Gould, Z. Cheng, B. Xu, B. Saha, D.G. Vlachos, Catalytic hydrodeoxygenation of highcarbon furylmethanes to renewable jet-fuel ranged alkanes over a rhenium-modified iridium catalyst, ChemSusChem 10 (2017) 3225–3234.
[21] Y. Takeda, T. Shoji, H. Watanabe, M. Tamura, Y. Nakagawa, K. Okumura, K. Tomishige, Selective hydrogenation of lactic acid to 1,2-propanediol over highly active ruthenium-molybdenum oxide catalysts, ChemSusChem 8 (2015) 1170–1178.
[22] K.H. Kang, U.G. Hong, Y. Bang, J.H. Choi, J.K. Kim, J.K. Lee, S.J. Han, I.K. Song, Hydrogenation of succinic acid to 1,4-butanediol over Re-Ru bimetallic catalysts supported on mesoporous carbon, Appl. Catal. A: Gen. 490 (2015) 153–162.
[23] Y. Takeda, M. Tamura, Y. Nakagawa, K. Okumura, K. Tomishige, Characterization of Re-Pd/SiO_2 catalysts for hydrogenation of stearic acid, ACS Catal. 5 (2015) 7034–7047.
[24] M. Jahandar Lashaki, A. Sayari, CO_2 capture using triamine-grafted SBA-15: the impact of the support pore structure, Chem. Eng. J. 334 (2018) 1260–1269.
[25] T.L.R. Hewer, A.G.F. Souza, K.T.C. Roseno, P.F. Moreira, R. Bonfim, R.M.B. Alves, M. Schmal, Influence of acid sites on the hydrodeoxygenation of anisole with metal supported on SBA-15 and SAPO-11, Renew. Energy 119 (2018) 615–624.
[26] P. Gaudin, L. Michelin, L. Josien, H. Nouali, S. Dorge, J.F. Brilhac, E. Fiani, M. Vierling, M. Moliere, J. Patarin, Highly dispersed copper species supported on

SBA-15 mesoporous materials for SO_x removal: Influence of the CuO loading and of the support, Fuel Process. Technol. 148 (2016) 1–11.
[27] G. Kresse, J. Hafner, Ab initio molecular dynamics for liquid metals, Phys. Rev. B: Condens. Matter Mater. Phys. 48 (1993) 13115–13118.
[28] G. Henkelman, B.P. Uberuaga, H. Jónsson, A climbing image nudged elastic band method for finding saddle points and minimum energy paths, J. Chem. Phys. 113 (2000) 9901–9904.
[29] F. Yang, N.J. Libretto, M.R. Komarneni, W. Zhou, J.T. Miller, X. Zhu, D.E. Resasco, Enhancement of m-cresol hydrodeoxygenation selectivity on Ni catalysts by surface decoration of MoO_x species, ACS Catal. 9 (2019) 7791–7800.
[30] J. Pritchard, A. Ciftci, M.W.G.M. Verhoeven, E.J.M. Hensen, E.A. Pidko, Supported Pt-Re catalysts for the selective hydrogenation of methyl and ethyl esters to alcohols, Catal. Today 279 (2017) 10–18.
[31] F. Yang, D. Liu, H. Wang, X. Liu, J. Han, Q. Ge, X.L. Zhu, Geometric and electronic effects of bimetallic Ni–Re catalysts for selective deoxygenation of m-cresol to toluene, J. Catal. 349 (2017) 84–97.
[32] S. Engels, J. Eick, W. Morke, U. Maier, I. Boszormenyi, K. Matusek, Z. Schay, L. Guczi, Characterization and catalytic activity of unsupported nickel-rhenium catalysts modified by calcium oxide, J. Catal. 103 (1987) 105–114.
[33] K. Liu, J. Pritchard, L. Lu, R. van Putten, M. Tiny Verhoeven, M. Schmitkamp, X. M. Huang, L. Lefort, C.J. Kiely, E.G.M. Hensen, E.A. Pidko, Supported nickel-rhenium catalysts for selective hydrogenation of methyl esters to alcohols, Chem. Commun. 53 (2017) 9761–9764.
[34] J. Yu, Y. Yang, L. Chen, Z. Li, W. Liu, E. Xu, Y.J. Zhang, S. Hong, X. Zhang, M. Wei, NiBi intermetallic compounds catalyst toward selective hydrogenation of unsaturated aldehydes, Appl. Catal. B: Environ. 277 (2020) 1–9.
[35] E. Kordouli, B. Pawelec, K. Bourikas, C. Kordulis, J.L.G. Fierro, A. Lycourghiotis, Mo promoted Ni-Al_2O_3 co-precipitated catalysts for green diesel production, Appl. Catal. B: Environ. 229 (2018) 139–154.
[36] X.C. Cao, F. Long, Q.L. Zhai, P. Liu, J.M. Xu, J.C. Jiang, Enhancement of fatty acids hydrodeoxygenation selectivity to diesel-range alkanes over the supported Ni-MoO_x catalyst and elucidation of the active phase, Renew. Energy 162 (2020) 2113–2125.
[37] P. Kumar, S.K. Maity, D. Shee, Role of NiMo alloy and Ni species in the performance of NiMo/alumina catalysts for hydrodeoxygenation of stearic acid: a kinetic study, ACS Omega 4 (2019) 2833–2843.
[38] Y. Takeda, Y. Nakagawa, K. Tomishige, Selective hydrogenation of higher saturated carboxylic acids to alcohols using a ReO_x-Pd/SiO_2 catalyst, Catal. Sci. Technol. 2 (2012) 2221–2223.
[39] S.Y. Xing, Y. Liu, X.C. Liu, M. Li, J.Y. Fu, P.F. Liu, P.M. Lv, Z.M. Wang, Solvent-free hydrodeoxygenation of bio-lipids into renewable alkanes over NiW bimetallic catalyst under mild conditions, Appl. Catal. B: Environ. 269 (2020) 1–11.
[40] Z. Luo, Q. Bing, J. Kong, J.Y. Liu, C. Zhao, Mechanism of supported Ru_3Sn_7 nanocluster-catalyzed selective hydrogenation of coconut oil to fatty alcohols, Catal. Sci. Technol. 8 (2018) 1322–1332.
[41] L.M. Martínez-Prieto, M. Puche, C. Cerezo-Navarrete, B. Chaudret, Uniform Ru nanoparticles on N-doped graphene for selective hydrogenation of fatty acids to alcohols, J. Catal. 377 (2019) 429–437.
[42] G. Xu, Y. Zhang, Y. Fu, Q. Guo, Efficient hydrogenation of various renewable oils over Ru-HAP catalyst in water, ACS Catal. 7 (2017) 1158–1169.
[43] J. Ni, W.H. Leng, J. Mao, J.G. Wang, J.Y. Lin, D.H. Jiang, X.N. Li, Tuning electron density of metal nickel by support defects in Ni/ZrO_2 for selective hydrogenation of fatty acids to alkanes and alcohols, Appl. Catal. B: Environ. 253 (2019) 170–178.
[44] J.M. Liang, Z.Y. Zhang, K.J. Wu, Y.C. Shi, W.H. Pu, M.D. Yang, Y.L. Wu, Improved conversion of stearic acid to diesel-like hydrocarbons by carbon nanotubes-supported CuCo catalysts, Fuel Process. Technol. 188 (2019) 153–163.
[45] P.J. Wang, Y. Jing, Y. Guo, Y. Cui, S. Dai, X.H.Y.Q. Liu, Y.Q. Wang, Highly efficient alloyed NiCu/Nb_2O_5 catalyst for the hydrodeoxygenation of biofuel precursors into liquid alkanes, Catal. Sci. Technol. 10 (2020) 4256–4263.
[46] N. Chen, Y. Ren, E.W. Qian, Elucidation of the active phase in PtSn/SAPO-11 for hydrodeoxygenation of methyl palmitate, J. Catal. 334 (2016) 79–88.